Angular Spectrum of Vortex Micro-lens

Seyyed Hossein Kazemi
Electrical Engineering Department, Quchan University of Technology, Quchan, Iran
Email: sh.kazemi@qiet.ac.ir

Ali Jebelli
Faculty of Engineering, University of Ottawa, Ottawa, Canada
Email: ajebelli@uottawa.ca

***Abstract*—Using the Angular Spectrum (AS) method, we have calculated the spatial distribution of the light intensity ring at the observation plane for a Vortex Micro-lens (VML). By comprehensive investigation of the variations in the ring characteristics, including the radius and width of the ring, the maximum intensity and the radius of the null spot versus the observation plane distance and VML topological charge, we have found a zone of maximum power level behind the VML in the Fresnel region. The zone is located at the between its double peaks. We call this zone the Maximum Power Zone (MPZ) and Also, we have shown that the location of the MPZ is independent of the refractive index and topological charge of VML while is dependent on frees-pace wavelength (λ_0) and diameter of VML (D) and there is an absolute peak of power level in the MPZ at the distance of $D^2/3\lambda_0$. The result can easily use to design a VML with a specified ring characterization.**

***Index Terms*—DOE, vortex micro-lens, angular spectrum and design**

I. Introduction

Vortex Micro-lens (VML) is a Diffractive Optical Element (DOE) that causes a spin in the transmitted wave polarization and generates a bright ring of light with a null spot in its center at the observation plane. This type of wave is suitable for telecommunications as it has self-healing property [1], [2]. VMLs are also used to couple modes from a single-mode optical fiber to a graded-index fiber [3]. Since the central null spot in a vortex wave has the ability to trap and spin particles, it is also used as an optical tweezer [4].

In addition to the vortex lens that we will investigate in this paper, other devices such as helical mirrors [5], dielectric wedges [6], spiral phase plates [7], spatial light modulators [8], spiral phase mirrors [9], and patch antennas [10], are also used to generate vortex waves. Devil's vortex-lenses [11] and plasmonic vortex lenses [12], which utilize fractal blazed profile and metal annular lines on a dielectric substrate respectively, are two other types of vortex lenses.

In this paper, we study the behavior of the intensity ring, generated by VML, and consider VML as a phase only element and use the angular spectrum method to compute the light distribution behind the lens. The structure of the paper is as follows. In Section 2, we introduce the problem geometry, define the characteristics of the bright ring and describe the angular spectral method briefly. We investigate the changes in the ring characteristics as a function of the observation plane distance and topological charge of VML in Section 3. This is followed by conclusions in Section 4.

II. Geometry of the Problem

A vortex lens is characterized by the dielectric refractive index, n, diameter, D, and topological charge, m. The phase profile of a VML sample with m = 5 is shown in Fig. 1. The discontinuity of the VLM profile is due to phase jumps at angles of $2\pi/m$ radians. The phase function of the transmitted wave is

$$\Phi(\varphi) = \mathrm{mod}_{2\pi}(m\varphi) \quad 0 \le \varphi \le 2\pi \quad m = 1,2,3,... \qquad (1)$$

where φ is the angle with the x axis in radians.

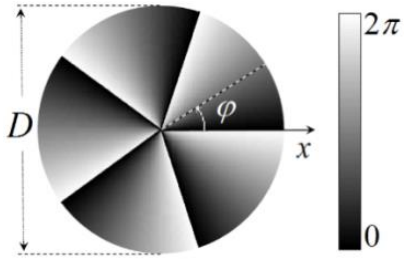

Figure 1. Phase profile, Φ (φ), of a vortex lens with m = 5.

The geometry of the problem is shown in Fig. 2(a). The input plane that includes the aperture is located in front of the VLM and the observation plane is located at $z = L$. It is assumed that a plane wave propagates along the z-axis and interacts with the VML at the input plane and produces the ring intensity pattern at the observation plane.

The space between the input and the observation plane - can be divided to two regions: VML region and Angular Spectrum (AS) region. The VML region extends from the input plane to the output plane (P_0) and includes VML, while the AS region extends from the output plane located at z = 0 to the observation plane (P_1). The thickness of VML region is equal to the maximum etch

Manuscript received August 20, 2019; revised November 8, 2019.

doi: 10.18178/joig.7.4.145-148

depth (d_{max} = $\lambda_0/(n - n_0)$). The refractive index of the dielectric material used is n, while the surrounding medium is assumed to be air (n_0 = 1). The transfer function of the VML is

$$t(x, y)= \tau \exp[\, j\Phi(\varphi)]circ(2r / D) \quad (2)$$

where $r = (x^2+y^2)^{½}$, $\tau = 2n_0/(n_0+n)$ is the Fresnel transmission coefficient, circ($2r/D$) is equal to 1 for any point inside a circular aperture of diameter D, and is equal to zero for other points. We assume an incident plane wave, $\boldsymbol{u}_{inc}$, that is propagating normal to the aperture. The wave at the output plane of the first region is $\boldsymbol{u}_0 = t(x,y)\ \boldsymbol{u}_{inc}$. The angular spectrum of $\boldsymbol{u}_0$, *i.e.*, $\boldsymbol{U}_0$, is defined as

$$\mathbf{U}_0(f_x, f_y) = \iint_{P_0} \mathbf{u}_0(x, y) \exp[-j2\pi(f_x x + f_y y)]dxdy \quad (3)$$

The field distribution in the observation plane, $\mathbf{u}_1$, can be obtained by

$$\mathbf{u}_1(x, y) = \iint \mathbf{U}_0 \mathrm{H}(f_x, f_y) \exp[\, j2\pi(f_x x + f_y y)]df_x df_y \quad (4)$$

where the transfer function, $H\ (f_x, f_y)$

$$\mathrm{H}(f_x, f_y) = \exp[\, jkL\sqrt{1-(\lambda\ f_x)^2 - (\lambda\ f_y)^2}\,] \quad (5)$$

In this equation, $k = nk_0$ and $\lambda = \lambda_0/n$ are the wave-number and wavelength inside the dielectric, respectively [13], [14].

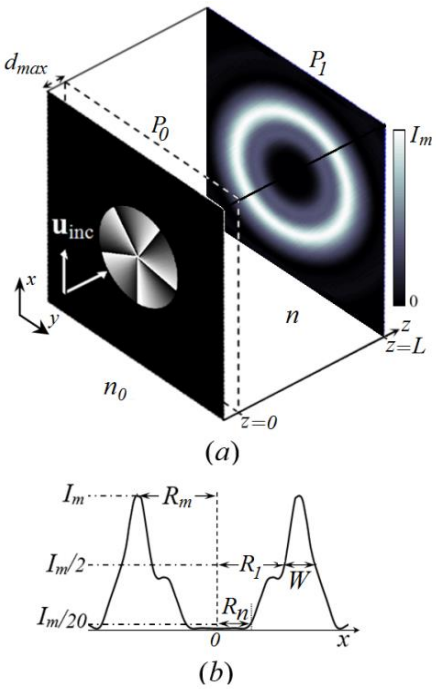

Figure 2. (*a*) Geometry of the problem illuminated by a plane wave, (*b*) the cross section of the light intensity distribution at the observation plane.

Fig. 2(b) shows a two-dimensional image of the light intensity distribution and its cross-sectuib in the observation plane. In this figure, R_m is the distance from the center of the ring to the location of the maximum intensity, I_m, and W is the main lobe width. The radius of the central null spot, R_n, is defined at intensity levels of $0.5I_m$ and $0.05I_m$. The radius of the bright ring is $R_r = R_1 + W/2$ which converges to R_m at the far field and its surface area is equal to $S_r = 2\pi R_r W$.

In the next section, we investigate the variations of I_m, R_m, W, R_n, and R_r versus L for different values of m. Since the intensity distribution in the near field, does not appear as a ring, we limit our analysis to the Fresnel region, *i.e.*, $L > 0.62(D^3/\lambda)^{½}$.

III. The Optical Ring Characteristics

Please Fig. 3(a) shows half of the cross section of the intensity distribution ring for VML with $D = 25\lambda_0$ and $m = 5$ at several distances of L = 200λ, 225λ, 250λ, and 275λ. As we can see, the first curve, corresponding to L = 200λ, has two slave and master peaks, marked with P_1 and P_2, respectively. By increasing the distance from 200λ to 225λ, the height of P_2 is decreased and moves away from the center which results in increasing of R_m. This can be considered as the normal behavior of the ring.

At L = 250λ, the heights of P_1 and P_2become equal and the intensity distribution curve becomes flat. For larger values of L, the height of P_1, exceeds P_2, and the value of R_m should be calculated from P_1. Therefore, R_m encounters a discontinuity or a sharp decrease. We call this exchange of master and slave peaks as abnormal behavior of the ring. By increasing the distance to L = 275λ, the normal behavior is resumed but for new master (P_1). Later, we will show that within the range of this abnormal behavior there is a zone with special characteristics.

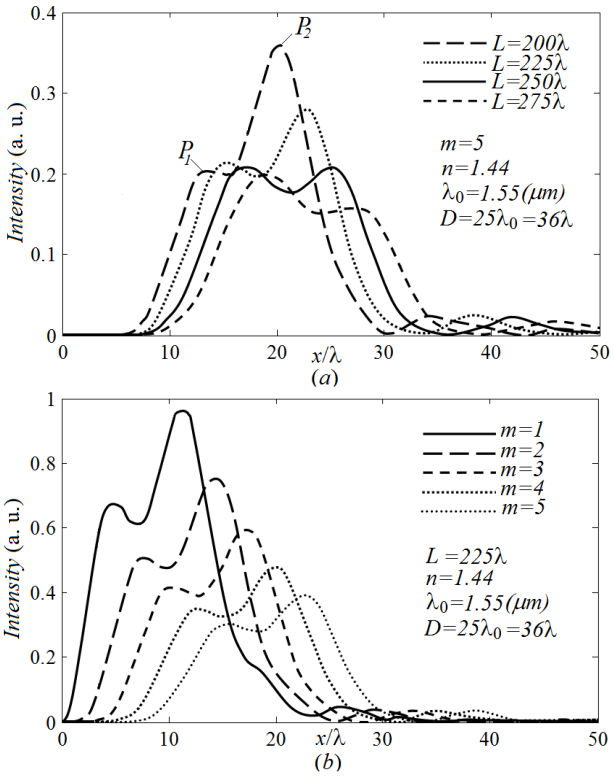

Figure 3. Cross-section of the intensity distribution of the light ring versus the normalized transverse distance x/λ for(a) several values of the distances from observation plane and m = 5 and (b) several values of m with constant distance L = 225λ.

Fig. 3(b) shows the effect of changing the topological charge m on the intensity distribution at $L = 225\lambda$. By increasing the topological charge, the values of R_n, R_m and W are increased while the maximum intensity is reduced.

Fig. 4 shows the changes in the radius of maximum intensity, the - maximum intensity, the ring width and the radius of the null spot versus the distance and topological charge. By dividing the distance (horizontal axis) by $L_p = D^2/3\lambda_0 = D^2/3n\lambda$, and dividing other ring characteristics, *i.e.*, R_m, W and R_n by $D\lambda$, these graphs are normalized to be used for each VML with arbitrary specifications, such as diameter, refractive index, and wavelength.

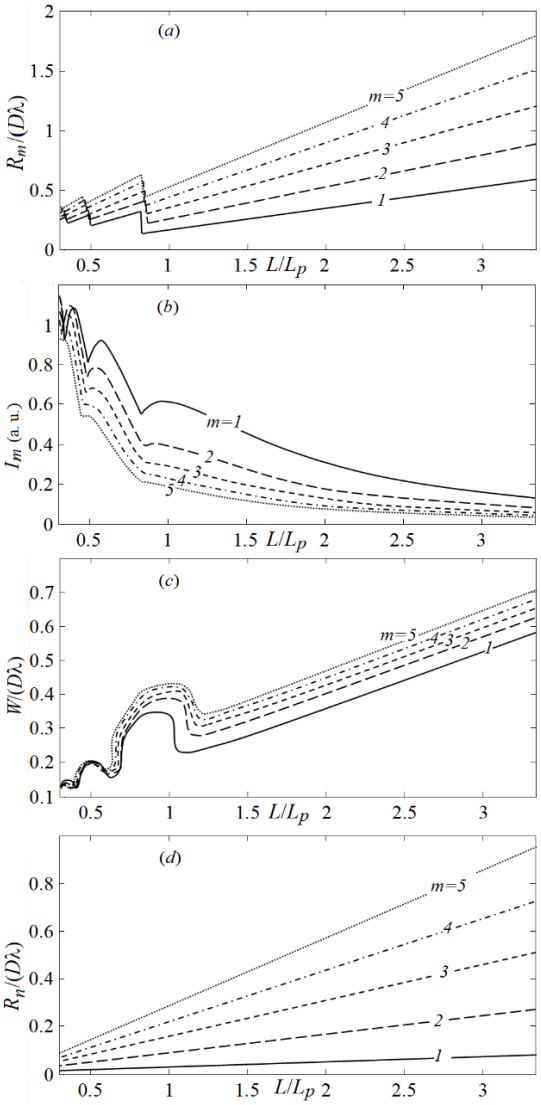

Figure 4. (*a*) The radius of maximum intensity, (*b*) the maximum intensity, (*c*) the ring width and (*d*) the radius of null spot, versus L/Lp for some values of m.

Fig. 4(a) shows that, except in three discontinuities, R_m is increased by increasing the distance and has normal behavior. These discontinuities (abnormal behavior), as shown in Fig. 3(a), are due to competition between the double peaks. This figure also shows that, although the slopes of the curves are increased with m, the positions of discontinuities are independent of m and are almost constant. Contrary to R_m, the radius of the ring, $R_r = R_1+W/2$, has no so discontinuity, and is approximately linear and has uniform behavior which converges to R_m in the far field.

Fig. 4(b) shows that increasing L and m, which results in increasing S_r, reduces the maximum intensity. But, this decrease is not uniform and at three positions that correspond to the local maxima of R_m in Fig. 4(a).

Fig. 4(c) shows - ring width, W, as a function of distance, L. In this figure, three local maximums that correspond to the three abnormal behavior of the ring are seen. This figure shows that after the last abnormal behavior, W *increases* steadily. As it can be seen in Fig. 4(c), the width, W, increases as m is increased. Fig. 4(d) shows the variations in the radius of the central null spot, R_n, in terms of L and m. This radius increases proportional to the value of m.

By defining the ring power as $P_m = S_r I_m$, we combine the information in Fig. 4 and provide a clear view in Fig. 5. This figure shows the distribution of power in the bright ring, and determines the Maximum Power Zone (MPZ) with an absolute maximum at $L = L_p$.

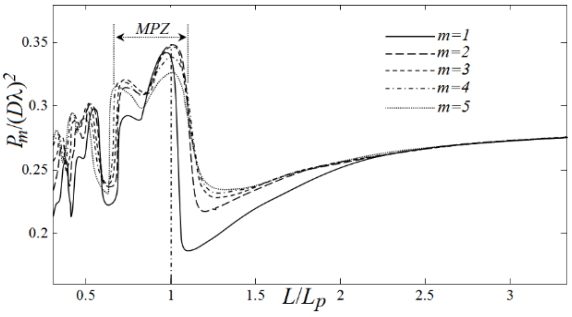

Figure 5. The power of the ring versus L/L_p for different values of m.

This zone, located at an approximate distance of $0.67L_p$ to $1.1L_p$, can be used to analyze or design VMLs. An increase in m causes a slight increase in the width of the MPZ, but has no significant effect on the position of the zone, its maximums and its dips. The positions of dips in MPZ correspond to the locations of maximum uniformity in the ring distribution (see Fig. 3(a)). Fig. 5 also shows that the far field zone of the VML starts at about $2L_p = 2D^2/3\lambda_0$.

At the end of this section, as an example, we use the information provided above to design a VML. Suppose we want to set the diameter and topological charge for a VML such that it converts a uniform light beam of wavelength $\lambda_0 = 1.55$ μm, into a skew beam to be coupled into a graded-index fiber. The radius of the central null spot is assumed to be $R_n = 5$ μm and VML will be fabricated on a silica substrate with a refractive index of $n_s = 1.44$ and a thickness of $L_s = 100$ μm.

To design this VML, we choose $L = L_p$ to obtain the maximum power at the input of the fiber. On the other hand, by reducing the maximum etch depth $d_{max} = 3.53$ μm, the substrate thickness is obtained, $L_p = L_s\text{-}d_{max} = 96.47$ μm, and hence the VML diameter is calculated as $D = (3\lambda_0 L_p)^{1/2} = 21.172$μm. Now, we can calculate the value of $R_n/(D\lambda) = 0.22$. Using this value and $L/L_p=1$, the topological charge is obtained from Fig. 4(d), *i.e.*, $m = 4$.

IV. Conclusions

In this paper, we provided an angular spectrum analysis of the - intensity ring of a VML. The graphs and analysis results are presented in such a way that can be used for any VML with any refractive index, diameter, and at arbitrary wavelength. We also have shown that at three distinct intervals, independent of the refractive index and topological charge of VML, the light intensity ring has three abnormal behaviors due to the phenomenon of competition between the double peaks and the last abnormal behavior determines the maximum power zone. Finally, using the specification of this zone, we designed a VML to couple uniform beam into a graded-index fiber as a skew beam.

References

[1] G. Gbur and R. K. Tyson, "Vortex beam propagation through atmospheric turbulence and topological charge conservation," *J. Opt. Soc. Am. A*, vol. 25, no. 1, pp. 225-230, 2008.

[2] G. Gibson, J. Courtial, M. Padgett, M. Vasnetsov, V. Pas'ko, S. Barnett, and S. Franke-Arnold, "Free-space information transfer using light beams carrying orbital angular momentum," *Opt. Express*, vol. 12, no. 22, pp. 5448-5456, 2004.

[3] E. G. Johnson, J. Stack, and C. Koehler, "Light coupling by a vortex lens into graded index fiber," *Journal of Lightwave Technology*, vol. 19, no. 5, pp. 753-758, 2001.

[4] D. McGolin, G. C. Spalding, H. Melville, W. Sibbett, and K. Dholakia, "Applications of spatial light modulators in atom optics," *Opt. Express*, vol. 11, no. 2, pp. 158-166, 2003.

[5] D. P. Ghai, P. Senthilkumaran, and R. S. Sirohi, "Adaptive helical mirror for generation of optical phase singularity," *Appl. Opt.*, vol. 47, no. 10, pp. 1378-1383, 2008.

[6] Y. Izdebskaya, V. Shvedov, and A. Volyar, "Generation of higher-order optical vortices by a dielectric wedge," *Opt. Lett.*, vol. 30, no. 18, pp. 2472-2474, 2005.

[7] S. S. R. Oemrawsingh, J. A. W. V. Houwelingen, E. R. Eliel, J. P. Woerdman, E. J. K. Verstegen, J. G. Kloosterboer, and G. W. Thooft, "Production and characterization of spiral phase plates for optical wavelengths," *Appl. Opt.*, vol. 43, no. 3, pp. 688-694, 2004.

[8] D. McGloin, *et al*., "Atom guiding along high order Laguerre–Gaussian light beams formed by spatial light modulation," *J. Mod. Opt.*, vol. 53, no. 4, pp. 547-556, 2006.

[9] G. Campbell, B. Hage, B. Buchler, and P. K. Lam, "Generation of high-order optical vortices using directly machined spiral phase mirrors," *Appl. Opt.*, vol. 51, no. 7, pp. 873-876, 2012.

[10] J. Hu, T. Qiu, X. Lan, W. Xu, and S. Qian, "Three-Mode vortex wave generator with double-layer patch antennas," *International Journal of Antennas and Propagation*, vol. 2019, article ID 3737868, pp. 1-7, 2019.

[11] W. D. Furlan, F. Giménez, A. Calatayud, and J. A. Monsoriu, "Devil's vortex-lenses," *Opt. Express*, vol. 17, no. 24, pp. 21891-21896, 2009.

[12] H. Zhou, J. Dong, Y. Zhou, J. Zhang, M. Liu, and X. Zhang, "Designing appointed and multiple focuses with plasmonic vortex lenses," *IEEE Photonics Journal*, vol. 7, no. 4, p. 4801007, 2015.

[13] S. H. Kazemi, M. M. Mirsalehi, and A. R. Attari, "Comparison of angular spectrum angular spectrum and optimal rotation angle methods in designing beam-fanners," *Opt. Express*, vol. 17, no. 17, pp. 14825-14831, 2009.

[14] J. W. Goodman, *Introduction to Fourier Optics*, Englewood: Roberts & Company, 2005.

Seyyed Hossein Kazemi received B.Eng. degree in Electronic Engineering in 1997 from Yazd University, Iran. He received his Master and Ph.D. in Telecommunication Engineering from Ferdowsi University, Iran in 2000 and 2009. At present he is a Professor in the Electrical Engineering Department at the Quchan University of Technology, Iran.

Ali Jebelli received his Master's degree and Ph.D. in Electrical and Computer Engineering from the University of Ottawa in 2014 and 2016. During his studies at the University of Ottawa, he worked as a research assistant and teacher assistant in the Department of Mechanical Engineering and the School of Electrical Engineering and Computer Science, and during that time, he won several prestigious awards. He also received a Master degree (MEng) in Electrical–Mechatronics and Automatic Control from the University Technology Malaysia in 2009, and his bachelor's degree in Electrical Power Engineering from Azad University in 2005.